Journal of Nuclear Medicine, published on September 15, 2016 as doi:10.2967/jnumed.116.178939

Preclinical evaluation and first patient application of ^{99m}Tc-PSMA-I&S for SPECT imaging and radioguided surgery in prostate cancer

Stephanie Robu[1§], Margret Schottelius[1§*], Matthias Eiber[2], Tobias Maurer[3], Jürgen Gschwend[3], Markus Schwaiger[2] and Hans-Jürgen Wester[1]

[1] Chair of Pharmaceutical Radiochemistry, Technische Universität München, Walther-Meissner-Strasse 3, 85748 Garching, Germany

[2] Department of Nuclear Medicine, Klinikum rechts der Isar, Technische Universität München, Ismaningerstr. 22, 81675 München, Germany

[3] Department of Urology, Klinikum rechts der Isar, Technische Universität München, Ismaningerstr. 22, 81675 München, Germany

* to whom correspondence should be addressed

Stephanie Robu
Chair for Pharmaceutical Radiochemistry
Technische Universität München
Walther-Meissner-Str. 3
85748 Garching
Germany
Phone: +49 89 289 12203
Fax: +49 89 289 12204
stephanie.robu@tum.de

[§] Stephanie Robu and Margret Schottelius contributed equally to this work

Word count of the manuscript: 5945

[^{99m}Tc]PSMA-I&S for RGS and SPECT

ABSTRACT

Initial studies in patients have demonstrated the suitability of ^{111}In-PSMA-I&T (^{111}In-DOTAGA-(3-iodo-y)-f-k-Sub(KuE)) for radioguided surgery (RGS) of small metastatic prostate cancer (PCa) soft tissue lesions. To meet the clinical need for a more cost-effective alternative, the PSMA-I&T-based tracer concept was adapted to ^{99m}Tc-labeling chemistry. Two PSMA-I&T-derived inhibitors with all-L-serine- (MAS_3) and all-D-serine- (mas_3) chelating moieties were evaluated in parallel, and a kit procedure for routine ^{99m}Tc-labeling was developed.

Methods: PSMA-affinities (IC_{50}) and internalization kinetics of ^{99m}Tc-MAS_3-y-nal-k(Sub-KuE) and ^{99m}Tc-mas_3-y-nal-k(Sub-KuE) ("^{99m}Tc-PSMA-I&S" for **I**maging and **S**urgery) were determined using LNCaP cells and (^{125}I-BA)KuE as radioligand and reference standard. *In vivo* metabolite analyses and biodistribution studies were carried out using CD-1 nu/nu and LNCaP-tumor bearing CB-17-SCID mice. Pharmacokinetics of ^{99m}Tc-PSMA-I&S in humans were investigated in a patient with advanced metastatic PCa via sequential planar whole-body SPECT imaging at 1, 3, 5 and 21h p.i. Additionally, preoperative SPECT/CT (12h p.i.) and ^{99m}Tc-PSMA-I&S-supported RGS (16h p.i.) were performed in one PCa patient with proven iliac and inguinal lymph node metastases.

Results: A robust and reliable kit-labeling procedure was established, allowing the preparation of ^{99m}Tc-MAS_3-y-nal-k(Sub-KuE) and ^{99m}Tc-PSMA-I&S in consistently high radiochemical yield and purity ($\geq$98%, n>50 preparations). Because of its improved internalization efficiency and superior *in vivo* stability, ^{99m}Tc-PSMA-I&S was selected for further *in vivo* evaluation. Compared to ^{111}In-PSMA-I&T, ^{99m}Tc-PSMA-I&S showed delayed clearance kinetics, but identical uptake in PSMA$^+$ tissues in the LNCaP xenograft model (1h p.i.). In exemplary PCa patients, relatively slow whole-body clearance of ^{99m}Tc-PSMA-I&S was also observed due to high plasma protein binding (94%) of the tracer. This, however, promoted efficient tracer uptake in PCa lesions over time, and lead to steadily increasing lesion-to-background ratios up to 21h p.i.. Preoperative SPECT/CT showed high ^{99m}Tc-PSMA-I&S uptake in all suspect lesions identified in previous

^{68}Ga-HBED-CC-PSMA PET/CT, allowing for their successfully intraoperative detection and resection during first-in-man RGS.

Conclusion: Due to a straightforward and reliable kit-production, ^{99m}Tc-PSMA-I&S represents a cost-effective, readily available alternative to ^{111}In-PSMA-I&T. Initial patient data indicate its comparable or even superior performance as a probe for PSMA-targeted RGS and also hint towards the unexpected potential of ^{99m}Tc-PSMA-I&S as a SPECT imaging agent.

Key Words:

PSMA, ^{111}In-PSMA-I&T, ^{99m}Tc-PSMA-I&S, SPECT, gamma probe, radioguided surgery, RGS

INTRODUCTION

Recently, prostate-specific membrane antigen (PSMA) has emerged as one of the most extensively investigated and exploited targets for molecular imaging and radioligand therapy of prostate cancer (PCa). Because of its strong upregulation in PCa and low basal expression in non-prostatic tissues as well as the direct correlation between PSMA expression levels and androgen independence, metastasis and PCa progression (*1, 2*), PSMA reprensents a highly valuable molecular marker in PCa .

Therefore, intense efforts have been directed towards the development of PSMA-targeted probes for a variety of clinical applications ranging from diagnostic imaging using SPECT, PET, magnetic resonance imaging (MRI) or optical methods towards innovative theranostic and therapeutic concepts (*3, 4, 5, 6*).

With respect to clinical diagnostic imaging, the field was pioneered by small urea-based tracers such as ^{99m}Tc-MIP-1404 and ^{99m}Tc-MIP-1405 for SPECT (*7, 8*) as well as by ^{68}Ga-HBED-CC-Ahx-KuE (^{68}Ga-HBED-CC-PSMA) (*9, 10, 11*) or the ^{18}F-labeled analogs ^{18}F-DCFBC (*12, 13*) and ^{18}F-DCFPyl (*14, 15*) for PET. Their use for PET/CT or PET/MRI hybrid imaging has been shown to allow detection and characterization of primary and recurrent metastatic PCa, even at very low PSA levels, with higher sensitivity, specificity, and accuracy than conventional imaging methods (*16, 17, 18*).

Furthermore, several alternative theranostic approaches have been realized recently, providing versatile molecular platforms for labeling with diagnostic (^{123}I/^{124}I, ^{68}Ga) and therapeutic radionuclides (^{131}I, ^{177}Lu). Initial data on endoradiotherapeutic applications of ^{131}I-MIP-1095 (*19*), ^{177}Lu-DKFZ-617 (*20, 21*) and ^{177}Lu-PSMA-I&T (*22, 23*) in patients with metastatic PCa demonstrate comparable and highly promising molecular and morphological treatment responses for all three compounds (*3*). In addition, the concept of PSMA-targeted therapy can be expanded beyond endoradiotherapy towards radioguided surgery (RGS), as recently demonstrated by the introduction of [^{111}In]PSMA-I&T (*24, 25*). Preoperative injection of ^{111}In-PSMA-I&T was shown to substantially facilitate the intraoperative detection and resection of even small and atypically localized PSMA-positive metastatic lymph node deposits. In a small cohort of patients with

primary metastasized or early recurrent PCa, ^{111}In-PSMA-I&T-supported RGS allowed quantitative resection of all suspect lesions previously identified in ^{68}Ga-HBED-CC-PSMA PET/CT. Furthermore, ^{111}In-PSMA-I&T also showed reasonable *in vivo* performance as a PSMA-targeted imaging probe in pre-therapeutic SPECT/CT imaging at 4 h p.i. (*24, 25*). However, its suboptimal nuclear properties, the high cost and the limited availability of $^{111}InCl_3$ restricts the routine clinical application of ^{111}In-PSMA-I&T for PSMA-targeted RGS. To circumvent these issues, the development of a corresponding ^{99m}Tc-labeled analog seemed the conclusive next step. Here, major focus was directed towards the selection of a ^{99m}Tc-labeling strategy that ensures fast and robust radiolabeling and a straightforward translation into a kit formulation for clinical application.

To adapt the PSMA-I&T based theranostic concept to the requirements of ^{99m}Tc labeling, the DOTAGA-chelator in PSMA-I&T was replaced by mercaptoacetyl triserine, named "MAS_3" (*26, 27*). Furthermore, the 3-iodo-D-Tyr-D-Phe-sequence in the linker unit was replaced by D-Tyr-D-2-Nal to enhance interaction of the peptidic linker unit with a remote arene binding site (Fig. 1). Based on earlier work that had demonstrated the metabolic instability of the peptidic linker in DOTAGA-FFK-Sub-KuE (*28*), we hypothesized, that the all-L-amino acid chelator MAS_3 (2-mercaptoacetyl-Ser-Ser-Ser-) might also be susceptible towards proteolytic degradation. To investigate this hypothesis, the corresponding mas_3 (2-mercaptoacetyl-D-Ser-D-Ser-D-Ser-) analog (PSMA-I&S (for **I**maging and **S**urgery)) was also synthesized and evaluated in parallel.

FIGURE 1

METHODS

General

All animal experiments were conducted in accordance with the German Animal Welfare Act (Deutsches Tierschutzgesetz, approval no. 55.2-1-54-2532-71-13). All human studies were approved by the institutional review boards of the participating medical institutions. Patients provided signed informed consent.

Synthesis and Radiolabeling

The synthesis of MAS_3/mas_3-y-nal-k(Sub-KuE) was performed in analogy to a previously published protocol (*28*) with minor modifications (Figure 1). A detailed description of the ^{99m}Tc-labeling protocol is supplied in the supplemental data (available at http://jnm.snmjournals.org). The radioiodinated reference ligand (^{125}I-BA)KuE ((S)-1-carboxy-5-(4-(-^{125}I-iodo-benzamido)pentyl)carbamoyl)-L-glutamic acid) was prepared as described previously (*28*).

Lipophilicity and Plasma Protein Binding

The n-octanol/PBS partition coefficients of ^{99m}Tc-PSMA-I&S and ^{99m}Tc-MAS_3-y-nal-k(Sub-KuE) were determined as described using a shake-flask method (*28*). Log $P_{O/PBS}$ values were calculated from the means of n=6 separate determinations. The fraction of plasma protein bound tracer was determined by incubation of fresh human plasma samples with ^{99m}Tc-PSMA-I&S and ^{99m}Tc-MAS_3-y-nal-k(Sub-KuE), respectively (30 min, 37°C), and subsequent ultracentrifugation in VWR Centrifugal Filters (PES, 30K; VWR, Ismaning, Germany). The fraction of free ^{99m}Tc-inhibitor in plasma is defined as the ratio between the activity in the ultrafiltrate and in the unfiltered plasma sample. Values for plasma protein binding are corrected for nonspecific binding to the filter material.

In Vitro Studies

$PSMA^+$ LNCaP cells (CLS: 300265) were cultivated in DMEM/Nutrition Mix F-12 with Glutamax-I (1:1) (Invitrogen, Life Technologies, Darmstadt, Germany) supplemented with 10% FCS and were maintained at

37°C in a 5% CO_2/humidified air atmosphere. For IC_{50} determination, 150.000 cells/well were seeded in conventional 24-well plates one day prior to the experiment. For internalization studies, 125.000 cells/well and PLL-coated 24-well plates were used.

PSMA affinities (IC_{50}) were determined in a competitive binding assay using LNCaP cells and (^{125}I-BA)KuE as the radioligand (*28*). Data represent means ± standard deviation (± SD) of n≥3 separate determinations.

PSMA-specific ligand internalization kinetics were determined by incubation of LNCaP cells (37°C, 5, 15, 30 and 60 min, respectively) with the respective radioligands (0.2 nM) in the absence (total internalization) and presence (non-specific internalization) of 10 µM 2-PMPA (2-(phosphonomethyl)pentane-1,5-dioic acid). Data were corrected for non-specific internalization and normalized to the specific internalization observed for the reference compound (^{125}I-BA)KuE in a parallel experiment (*22*). Data are means ± SD (n = 3).

Metabolite Analyses

Approximately 20 MBq of the ^{99m}Tc-labelled tracers (0.5 – 0.6 nmol; specific activity 36 GBq/µmol) were injected into the tail vein of CD-1 nu/nu mice. At 1h postinjection, animals were sacrificed, blood and urine were collected, and kidneys were dissected. Sample preparation and reversed-phase high performance liquid chromatography (RP-HPLC) analysis were performed in analogy to a previous protocol (*28*) using a Chromolith Performance RP-18e column (100x4.6 mm; flow rate: 3 mL/min; Gradient: 3%B for 3min, 3% to 95%B in 6min, 95%B for 3min; solvent A: 0.1%TFA in water, solvent B: 0.1% TFA in acetonitrile).

In Vivo Biodistribution Studies

To induce LNCaP tumor growth, CB17 severe combined immunodeficiency (SCID) mice (6-8 weeks, male, Charles River Laboratories, Sulzfeld, Germany) were inoculated subcutaneously with approximately $1 \cdot 10^7$ LNCaP cells in 100 µL serum-free medium and 100 µL Matrigel (BD Biosciences, Germany). After an average

of 4-6 weeks, tumor size reached 4-8 mm in diameter, and the animals were used for biodistribution studies.

Biodistribution. About 3-4 MBq ^{99m}Tc-PSMA-I&S (0.1 nmol) or 1.5 MBq ^{111}In-PSMA-I&T (0.2 nmol) (*24*) were injected into the tail vein of the animals (n=5) under isoflurane anesthesia. For competition experiments, 2-PMPA (1 µmol=226 µg/mouse) was coinjected (n=3). Animals were sacrificed at 1h p.i., the organs of interest were dissected, and the activity in the weighed tissues samples was quantified using a γ-counter.

^{99m}Tc-PSMA- I&S Imaging and RGS in Patients

Diagnostic ^{68}Ga-HBED-CC-PSMA PET/CT-imaging of both PCa patients in this study was performed as described recently (*10*).

In one patient, whole-body scintigraphy and SPECT/CT were performed 1, 3, 5 and 21 hours after intravenous administration of 497 MBq ^{99m}Tc-PSMA-I&S on a Siemens Symbia T 6. Planar whole body images were acquired with continuous table feed of 10 cm/min, immediately followed by SPECT/CT acquisition. The SPECT acquisition (64x64 matrix, 64 frames, 30s/frame) was performed using 6 angular steps in a 20s time-frame. For CT (130 kV, 15 mAs), 5-mm slices were obtained.

First-in-man RGS was performed on one patient with primary metastatic prostate cancer 16h after intravenous injection of 607 MBq ^{99m}Tc-PSMA-I&S. After preoperative SPECT/CT 12h p.i. metastatic lymph nodes were detected intraoperatively using a gamma probe (Crystal Probe CXS-SG603, Crystal Photonics, Berlin, Germany).

RESULTS

Chemical Synthesis

The synthesis of the novel PSMA-I&T derived ligands is summarized in Scheme 1. Due to a greater ease of synthesis and better synthetic availability, $Sub(OPfp)_2$ (suberic acid bis-pentafluorophenyl ester) was used to prepare the protected linker-conjugated inhibitor component $(OtBu)K(Sub\text{-}OPfp)uE(OtBu)_2$ (**2**) in 68% yield based on **1**. Upon reaction with the respective protected peptidic linker units **3** and **4** that had been prepared via standard solid phase peptide synthesis in sufficient purity to allow immediate use for further reaction, the conjugates were deprotected and purified using preparative RP-HPLC. The final labeling precursors **5** and **6** were obtained in 71% and 63% yield, respectively, based on chelator-conjugated peptide spacer. The ^{nat}Re-complexes of **5** and **6** were synthesized under weakly acidic conditions using $KReO_4$ and $SnCl_2$ (90°C, 1h). To remove excess salts, Re-**5** and Re-**6** were purified using RP-HPLC. The identity of all final products was confirmed by ESI-MS.

Figure 2

^{99m}Tc-Labeling

For initial ^{99m}Tc-labeling experiments, a standard "wet chemistry" MAG_3 labeling procedure (*29*) was adapted to the requirements for the production of high specific activity radiopharmaceuticals by using only 20-30 nmol of labeling precursors **5** and **6**, respectively. Both for ^{99m}Tc-**5** (^{99m}Tc-PSMA-I&S) and ^{99m}Tc-**6**, no free [^{99m}Tc]pertechnetate was detected in the reaction mixture after heating the respective precursor and ^{99m}Tc-pertechnetate (1000-1200 MBq) for 20 min to 90°C in the presence of stannous chloride, ascorbic acid, tartrate and ammonium acetate (pH 7.5-8). However, substantial amounts (10-30% of added activity) of colloidal ^{99m}Tc species were detected in the respective preparations, necessitating a cartridge purification of ^{99m}Tc-PSMA-I&S and ^{99m}Tc-**6**, which were obtained in specific activities of 25-37 GBq/µmol.

Subsequently, the composition of the initial "wet chemistry" labeling mixture was adapted to the requirements for kit formulation. Thus, the volatile ammonium acetate buffer (pH=8) was replaced by phosphate buffer (pH=8), and single-dose freeze-dried kits containing 25 nmol of PSMA-I&S were prepared. As observed in the initial labeling studies, radiochemical yield of ^{99m}Tc-PSMA-I&S was also limited to 65–87% (n=5) in the kit preparations due to the formation of colloidal ^{99m}Tc species. Neither increasing the amount of labeling precursor nor adding a freshly prepared $SnCl_2$ solution to the kit immediately before the addition of ^{99m}Tc-pertechnetate nor using a higher amount of the reducing agent (50 µg) $SnCl_2$ or addition of ethanol to the kit reaction mixture (*30*) repressed ^{99m}Tc-colloid formation, whereas adjustment of the tartrate content in the lyophilized kits allowed the production of ^{99m}Tc-PSMA-I&S in consistently high radiochemical yield and radiochemical purity of ≥99% (n>50 kit preparations), with negligible formation ^{99m}Tc colloid (≤1% of added ^{99m}Tc-activity). The kit preparation of ^{99m}Tc-PSMA-I&S was found to be highly tolerant towards concentration and volume changes (1-10 ml reaction volume), affording ^{99m}Tc-PSMA-I&S in improved specific activities of 44–52 GBq/µmol.

Based on these findings, the cartridge purification step after ^{99m}Tc-labeling can safely be omitted. The synthesis is completed by dilution with sterile isotonic saline and sterile filtration.

In Vitro Evaluation

The PSMA affinities (IC_{50}) of the precursors **5** and **6** and of the corresponding ^{nat}Re-complexes of **5** and **6** were determined in a competitive binding assay using LNCaP human PCa cells and (^{125}I-BA)KuE (*31*) as the radioligand (0.2 nM; Table 1).

Both in the free and in the Re-complexed form, the novel MAS_3/mas_3-y-nal-k(Sub-KuE) analogs exhibit very similar PSMA affinities, indicating a negligible influence of the D- vs L-conformation of the serine residues in the mas_3/MAS_3 chelators as well as of the amino acid composition of the peptidic linker

(y-nal-k versus (3-iodo-y)-f-k in PSMA-I&T) on PSMA affinity. Compared to the reference compound ^{nat}In-PSMA-I&T, both Re-PSMA-I&S (Re-**5**) and Re-**6** show slightly reduced affinities towards PSMA.

TABLE 1

However, marked differences in the internalization efficiencies of ^{99m}Tc-PSMA-I&S (^{99m}Tc-**5**) (Fig. 3) and ^{99m}Tc-MAS$_3$-y-nal-k(Sub-KuE) ([^{99m}Tc]-**6**), were observed. Compared to ^{99m}Tc-**6**, ^{99m}Tc-PSMA-I&S showed enhanced internalization into LNCaP cells, which almost reaches the values obtained for ^{111}In-PSMA-I&T, whereas the internalization of ^{99m}Tc-**6** is substantially lower and comparable to that of ^{177}Lu-PSMA-I&T.

FIGURE 3

Lipophilicity and Plasma Protein Binding

The lipophilicites of ^{99m}Tc-PSMA-I&S and ^{99m}Tc-**6** are summarized in Table 1. Compared to the highly hydrophilic PSMA-I&T analogs, lipohilicity of the novel ^{99m}Tc-labeled compounds, albeit still very low, is increased by an order of magnitude.

The fraction of protein-bound tracer (human plasma) was found to be 94% and 95% for ^{99m}Tc-PSMA-I&S and ^{99m}Tc-**6**, respectively, which is considerably higher than the value observed for ^{111}In-PSMA-I&T (83%) (*24*).

In Vivo Metabolite Analysis

The *in vivo* metabolic stability of ^{99m}Tc-PSMA-I&S and ^{99m}Tc-**6** was investigated in CD-1 mice (Fig. 4). As expected, no *in vivo* degradation was observed for the stabilized analog ^{99m}Tc-PSMA-I&S, whereas

substantial radiometabolite formation was observed for ^{99m}Tc-**6** containing the L-amino acid MAS_3-chelator. In blood and urine, the percentage of intact ^{99m}Tc-**6** after 1h was only 52% and 88%, respectively, whereas no tracer degradation was observed in kidney. This suggests predominant metabolism of ^{99m}Tc-**6** in plasma and fast renal excretion of the radiometabolite.

FIGURE 4

Biodistribution

Given the superior metabolic stability of ^{99m}Tc-PSMA-I&S, only this tracer was further investigated in an *in vivo* biodistribution study (Table 2). As expected from its pronounced plasma protein binding, ^{99m}Tc-PSMA-I&S shows delayed blood clearance and thus increased blood and background activity levels compared to ^{111}In-PSMA I&T at 1h p.i.. The reduced hydrophilicity of ^{99m}Tc-PSMA-I&S leads to enhanced tracer uptake in liver and intestines, indicating an increased contribution of hepatobiliary clearance to overall tracer excretion. Interestingly, tracer accumulation in PSMA-expressing tissues, i.e. spleen, kidney and the LNCaP xenograft, is identical for both ^{99m}Tc-PSMA-I&S and ^{111}In-PSMA-I&T. This underlines the *in vitro* results (Table 1) that had already shown comparable PSMA targeting efficiencies for both compounds. PSMA-specificity of ^{99m}Tc-PSMA-I&S accumulation was confirmed by a competition study using a 1000-fold molar excess of the potent PSMA inhibitor PMPA (Table 2). Here, PSMA-mediated ^{99m}Tc-PSMA-I&S uptake in spleen, kidney and tumor was reduced to 3%, 5% and 22% of the tissue accumulation under “tracer only” conditions, respectively.

TABLE 2

First patient application of ^{99m}Tc-PSMA-I&S for SPECT Imaging and RGS

Based on these *in vivo* data, a first-in-man RGS study was carried out. To investigate tracer kinetics and to identify suitable time points for preoperative SPECT imaging and subsequent RGS, a 73 year-old patient with metastatic castration-resistant PCa was sequentially imaged over a total of 21 h (Fig. 4). Analogous to a prior ^{68}Ga-HBED-CC PSMA PET/CT scan (Fig. 5A), ventral and dorsal ^{99m}Tc-PSMA-I&S whole-body planar scintigraphies (Fig. 5B-E) revealed diffuse bone and lymph node metastases as early as 1 h p.i. (Fig. 5B). As expected from the preclinical data, ^{99m}Tc-PSMA-I&S showed delayed whole body clearance and efficient accumulation in PSMA expressing tissue (Fig. 5D). Although ^{99m}Tc-PSMA-I&S shows some diffuse uptake in liver and the gastrointestinal tract, most of the tracer is cleared from these and other organs within the observation period. In contrast, ^{99m}Tc-PSMA-I&S uptake in parotid and salivary glands and “PSMA-mediated” uptake in kidney as well as bone and lymph node metastases increases between 1 and 3 h p.i. and remains persistently high. These combined effects lead to gradually increasing lesion-to-background ratios up to 21 h p.i. (Fig. 5E).

FIGURE 5

Another patient (72 y), presenting with histologically confirmed primary prostate cancer (Gleason score 7b, pT2v, cNx, Mx, initial PSA 13 ng/ml) initially underwent ^{68}Ga-HBED-CC-PSMA PET/MR for pre-therapeutic staging. PET/MR showed iliac and atypically localized inguinal lymph node metastases with intense ^{68}Ga-HBED-CC-PSMA uptake (Fig. 6). The patient was subsequently scheduled for RGS. ^{99m}Tc-PSMA-I&S SPECT/CT images at 12h p.i. revealed intense PSMA-uptake in all previously identified lesions (^{68}Ga-HBED-CC-PSMA PET/MR), facilitating intraoperative identification of the suspect lymph nodes. The presence of PSMA-positive tumor tissue in the resected specimens was confirmed histopathologically after RGS.

FIGURE 6

DISCUSSION

The recent introduction of ^{111}In-PSMA-I&T for PSMA-targeted RGS and optional preoperative SPECT imaging has further widened the scope of current PSMA-directed theranostic concepts. However, the inherent limitations associated with ^{111}In as a radionuclide prevent the broader clinical use of ^{111}In-PSMA-I&T beyond proof-of-concept studies in small patient cohorts. Thus, the aim of this study was to adapt the general tracer concept to the requirements of ^{99m}Tc-chemistry.

The PSMA-I&T scaffold is tolerant towards structural modifications in the N-terminal region of the peptidic linker unit without pronounced effects on PSMA affinity (*22, 28*). Therefore, the different well established ^{99m}Tc-labeling methodologies such as HYNIC-, $^{99m}Tc(CO)_3^+$- and MAG_3-based strategies seemed equally well suited for the design of novel ^{99m}Tc-labeled PSMA-inhibitors. In addition, robust and reliable kit procedures have been developed (*32, 33, 34*) for these approaches, and the choice of suitable chelators or coligand systems allows finetuning of ligand pharmacokinetics via adjustment of hydrophilicity (*27*). MAG_3-based ^{99m}Tc-labeling approaches, however, have the advantage of neither requiring additional coligands for ^{99m}Tc-complexation (as opposed to HYNIC-functionalized precursors) nor necessitating the synthesis of complex chelator systems (as opposed to $^{99m}Tc(CO)_3^+$-chelation). The use of the hydrophilic MAG_3-analog MAS_3 (mercaptoacetyl-seryl-seryl-serine) leads to the formation of a well defined, hydrophilic ^{99m}Tc-complex while maintaining the ease and efficiency of the MAG_3 ^{99m}Tc-labeling procedure (*26*).

These features prompted the integration of MAS_3 into our PSMA-I&T based tracer design (Fig. 1). To the best of our knowledge, the potential influence of MAS_3 stereochemistry on ^{99m}Tc-labeling and stability of the corresponding ^{99m}Tc-radiopharmaceuticals has not been investigated so far. Thus, to close this gap, both the PSMA inhibitor bearing the all-L-serine- (MAS_3) and the all-D-serine- (mas_3) chelator (^{99m}Tc-**6** and ^{99m}Tc-PSMA-I&S (^{99m}Tc-**5**), respectively) were evaluated in parallel.

No detectable influence of chelator stereochemistry on the outcome of the ^{99m}Tc-labeling reaction was observed, since the formation of the ^{99m}TcO-MAS_3/mas_3-complex should be independent from the spatial orientation of the serine side chains. As hypothesized, however, based on the intrinsic susceptibility of L-amino acid peptides towards *in vivo* degradation by endopeptidases, the MAS_3 analog ^{99m}Tc-**6** showed substantially decreased *in vivo* stability compared to the mas_3-derivative ^{99m}Tc-PSMA-I&S, for which only intact tracer was detected in blood, urine and kidney at 1h p.i. (Fig. 4). In the case of ^{99m}Tc-**6**, rapid formation a hydrophilic radiometabolite in blood was observed; this metabolite was not detected in the kidney homogenate, but in the urine, indicating efficient renal clearance. Although the identity of the radiometabolite was not further investigated, it seems probable that enzymatic cleavage of the scissile bond between D-Tyr and the first L-Ser residue of MAS_3 leads to the formation of free ^{99m}Tc-MAS_3, which –in analogy to MAG_3 in renal scintigraphy- is then readily filtered into the urine without non-specific retention in kidney.

The present study was focused on the development of a suitable ^{99m}Tc-labeled probe for PSMA-targeted RGS. Here, a high *in vivo* stability represents a major prerequisite. In the clinical setting, RGS is usually performed on the day after tracer injection for practical reasons (*35*). Its success primarily relies on high lesion-to-background contrast at the time of surgery rather than fast tracer kinetics. The high *in vivo* stability of ^{99m}Tc-PSMA-I&S ensures the prolonged availability of intact tracer in the circulation, which can be expected to lead to progressively increasing activity accumulation in PSMA-expressing lesions over time.

This effect may be further amplified by the higher plasma protein binding displayed by ^{99m}Tc-PSMA-I&S (Table 1). In human plasma, app. 94% of ^{99m}Tc-PSMA-I&S are protein-bound, while this fraction amounts to only 83% for ^{111}In-PSMA-I&T. This is mirrored in the biodistribution data for these two compounds (Table 2), where ^{99m}Tc-PSMA-I&S shows a seven-fold higher blood activity concentration at 1h p.i. compared to ^{111}In-PSMA-I&T. As early as 1 h p.i., however, this is not immediately reflected in enhanced

targeting of ^{99m}Tc-PSMA-I&S to PSMA-overexpressing tissues such as kidney and tumor. Both ^{99m}Tc-PSMA-I&S and ^{111}In-PSMA-I&T show identical uptake values in these tissues (Table 2). As demonstrated by the blocking experiment (Table 2), however, ^{99m}Tc-PSMA-I&S uptake in kidney and tumor is highly PSMA-specific.

Based on the promising *in vivo* data obtained for ^{99m}Tc-PSMA-I&S, sequential planar imaging (1-21 h p.i., Fig. 5) was performed in one exemplary patient to establish the pharmacokinetics of ^{99m}Tc-PSMA-I&S in humans and to identify a suitable time window for RGS, where optimal lesion-to-background contrast is achieved, but intraoperative activity detection is not yet compromised by the decay of ^{99m}Tc.

As anticipated, whole-body clearance of ^{99m}Tc-PSMA-I&S is comparably slow, leading to relatively late background clearance, especially in the abdominal region. In accordance with our assumptions, however, tracer accumulation in the previously identified PCa lesions is steadily increasing over time as a result of the prolonged availability of the intact tracer in the blood and its internalization into the PSMA-expressing tumor cells. At later points ≥ 5h p.i., excellent lesion-to-background ratios are obtained due to the synergistic effect of persistent ^{99m}Tc-PSMA-I&S uptake in tumor tissue and continuing clearance of background activity.

Based on these data, ^{99m}Tc-PSMA-I&S-supported RGS was performed at 16h p.i. in an exemplary patient. As demonstrated in Fig. 6, preoperative ^{99m}Tc-PSMA-I&S SPECT/CT (12h p.i.) revealed high focal activity accumulation in several lymph node metastases, allowing for exact intraoperative identification and resection during RGS. It is important to note, that, although prelimiary in nature, these first-in-man studies suggest improved performance of ^{99m}Tc-PSMA-I&S compared to ^{111}In-PSMA-I&T, especially with respect to absolute tracer uptake in PCa lesions and, consequently, imaging contrast in preoperative SPECT.

Of course, the primary focus in the development of ^{99m}Tc-PSMA-I&S was its adaptation to the requirements of RGS. Preoperative SPECT imaging was primarily performed to confirm sufficient tracer

uptake in all suspect lesions previously identified via ^{68}Ga-HBED-CC-PSMA PET and thus to ensure their detectability during RGS. Surprisingly, however, the quality of planar and SPECT images obtained with ^{99m}Tc-PSMA-I&S compares well to images obtained with alternative highly promising PSMA-targeted SPECT imaging agents such as ^{99m}Tc-MIP-1404 (^{99m}Tc-trofolastat) (*8*). Although the latter had displayed fundamentally different pharmacokinetics in LNCaP xenograft bearing nude mice, i.e. fast background clearance and slightly increased tumor accumulation (*36*), as well as substantially lower plasma protein binding (32%) (*34*), suitable imaging contrast in PCa patients is only obtained at time points ≥ 4h p.i. due to considerable hepatic and intestinal tracer accumulation (*8*). In this context, a further evaluation of ^{99m}Tc-PSMA-I&S with emphasis on its suitability as a SPECT imaging agent seems highly recommendable. If our preliminary data are confirmed, they may even support the notion of first-line diagnosis of metastasized PCa via SPECT imaging in centers, where PET is not available. It remains questionable, however, if the late imaging time points required for high-contrast PCa imaging using the currently available ^{99m}Tc-labeled PSMA ligands are compatible with the patient workflow in imaging centers.

With respect to availability and ease of tracer preparation, ^{99m}Tc-PSMA-I&S is fully compatible with everyday clinical workflow. As a result of this study, a robust and reliable freeze-dried kit is now available for routine production of ^{99m}Tc-PSMA-I&S, facilitating the distribution and on-site production of this radiopharmaceutical for clincial applications in urology (RGS) and nuclear medicine (SPECT).

CONCLUSION

Based on the preclinical and first patient data obtained in this study, ^{99m}Tc-PSMA-I&S is a superior substitute for ^{111}In-PSMA-I&T for PSMA-targeted RGS. Its high value for the intraoperative detection of small metastatic lesions in PCa patients during RGS is supported by the results of currently ongoing RGS-

studies in >40 patients, and may, alongside with continuous advances in gamma probe technology (*37*), help to support the progressive integration of the concept of PSMA-targeted RGS into the clinic.

Competing Interests

All authors declare no conflict of interest.

Author Contributions

S.R. carried out the synthesis, ^{99m}Tc-labeling and kit formulation of PSMA-I&S, performed the preclinical *in vitro* and *in vivo* studies as well as tracer synthesis for patient application and drafted the manuscript.

M.Scho. was involved in the design, the *in vitro* and *in vivo* evaluation of ^{99m}Tc-PSMA-I&S as well as the PSMA-I&S kit development, performed data evaluation and interpretation and wrote the manuscript.

M.E. carried out the proof-of-principle ^{99m}Tc-PSMA-I&S whole-body scintigraphy and SPECT/CT of the patients as well as image and data interpretation and revised the final manuscript.

T.M. established and performed radioguided surgery using ^{99m}Tc-PSMA-I&S and revised the final manuscript.

J.G. was involved in initiating and establishing the concept of radioguided surgery using ^{99m}Tc-PSMA-I&S and revised the final manuscript.

M.Schw. supported the clinical evaluation of ^{99m}Tc-PSMA-I&S, participated in data interpretation and in revising the final manuscript.

H.J.W. initiated the development and evaluation of the PSMA-I&T platform, participated in data interpretation, in writing the manuscript and in revising the final manuscript.

ACKNOWLEDGEMENTS

The authors thank Alexandra Bartel, Simone Loher and Sven Hintze for their excellent technical assistance. Furthermore, the authors thank Gregor Weirich for performing the histophathological analysis of the resected tissues. The current study was financially supported by the Deutsche Forschungsgemeinschaft (SFB824; subproject Z1).

REFERENCES

1. Wright GL, Grob BM, Haley C, et al. Upregulation of prostate-specific membrane antigen after androgen-deprivation therapy. *Urology.* 1996;48(2):326-334.
2. Perner S, Hofer MD, Kim R, et al. Prostate-specific membrane antigen expression as a predictor of prostate cancer progression. *Hum Pathol.* 2007;38(5):696-701.
3. Lutje S, Heskamp S, Cornelissen AS, et al. PSMA Ligands for Radionuclide Imaging and Therapy of Prostate Cancer: Clinical Status. *Theranostics.* 2015;5(12):1388-1401.
4. Evangelista L, Zattoni F, Rossi E, Karnes RJ, Lowe V. Early detection of prostate cancer relapse by biochemistry and diagnostic imaging. *Q J Nucl Med Mol Imaging.* 2015;59(4):359-373.
5. Kiess AP, Banerjee SR, Mease RC, et al. Prostate-specific membrane antigen as a target for cancer imaging and therapy. *Q J Nucl Med Mol Imaging.* 2015;59(3):241-268.
6. Maurer T, Eiber M, Schwaiger M, Gschwend JE. Current use of PSMA-PET in prostate cancer management. *Nat Rev Urol.* 2016;13(4):226-235.
7. Maresca KP, Hillier SM, Lu GL, et al. Small molecule inhibitors of PSMA incorporating technetium-99m for imaging prostate cancer: Effects of chelate design on pharmacokinetics. *Inorg Chim Acta.* 2012;389:168-175.
8. Vallabhajosula S, Nikolopoulou A, Babich JW, et al. 99mTc-labeled small-molecule inhibitors of prostate-specific membrane antigen: pharmacokinetics and biodistribution studies in healthy subjects and patients with metastatic prostate cancer. *J Nucl Med.* 2014;55(11):1791-1798.
9. Eder M, Schafer M, Bauder-Wust U, et al. Ga-68-Complex Lipophilicity and the Targeting Property of a Urea-Based PSMA Inhibitor for PET Imaging. *Bioconjugate Chem.* 2012;23(4):688-697.
10. Eiber M, Maurer T, Souvatzoglou M, et al. Evaluation of Hybrid Ga-68-PSMA Ligand PET/CT in 248 Patients with Biochemical Recurrence After Radical Prostatectomy. *J Nucl Med.* 2015;56(5):668-674.
11. Afshar-Oromieh A, Avtzi E, Giesel FL, et al. The diagnostic value of PET/CT imaging with the (68)Ga-labelled PSMA ligand HBED-CC in the diagnosis of recurrent prostate cancer. *Eur J Nucl Med Mol Imaging.* 2015;42(2):197-209.
12. Mease RC, Dusich CL, Foss CA, et al. N-[N-[(S)-1,3-dicarboxypropyl]carbamoyl]-4-[F-18]fluorobenzyl-L-cysteine, [F-18]DCFBC: A new imaging probe for prostate cancer. *Clin Cancer Res.* 2008;14(10):3036-3043.
13. Rowe SP, Gage KL, Faraj SF, et al. (1)(8)F-DCFBC PET/CT for PSMA-Based Detection and Characterization of Primary Prostate Cancer. *J Nucl Med.* 2015;56(7):1003-1010.
14. Chen Y, Pullambhatla M, Foss CA, et al. 2-(3-{1-Carboxy-5-[(6-[18F]fluoro-pyridine-3-carbonyl)-amino]-pentyl}-ureido)-pen tanedioic acid, [18F]DCFPyL, a PSMA-based PET imaging agent for prostate cancer. *Clin Cancer Res.* 2011;17(24):7645-7653.
15. Szabo Z, Mena E, Rowe SP, et al. Initial Evaluation of [(18)F]DCFPyL for Prostate-Specific Membrane Antigen (PSMA)-Targeted PET Imaging of Prostate Cancer. *Mol Imaging Biol.* 2015;17(4):565-574.
16. Maurer T, Gschwend JE, Rauscher I, et al. Diagnostic Efficacy of (68)Gallium-PSMA Positron Emission Tomography Compared to Conventional Imaging for Lymph Node Staging of 130 Consecutive Patients with Intermediate to High Risk Prostate Cancer. *J Urology.* 2016;195(5):1436-1442.
17. Rowe SP, Macura KJ, Ciarallo A, et al. Comparison of Prostate-Specific Membrane Antigen-Based 18F-DCFBC PET/CT to Conventional Imaging Modalities for Detection of Hormone-Naive and Castration-Resistant Metastatic Prostate Cancer. *J Nucl Med.* 2016;57(1):46-53.
18. Eiber M, Weirich G, Holzapfel K, et al. Simultaneous Ga-PSMA HBED-CC PET/MRI Improves the Localization of Primary Prostate Cancer. *Eur Urol.* 2016.
19. Zechmann CM, Afshar-Oromieh A, Armor T, et al. Radiation dosimetry and first therapy results with a (124)I/ (131)I-labeled small molecule (MIP-1095) targeting PSMA for prostate cancer therapy. *Eur J Nucl Med Mol Imaging.* 2014;41(7):1280-1292.

20. Benesova M, Kratochwil C, Schafer M, et al. PSMA-617-a novel theranostic PSMA inhibitor for both diagnosis and endoradiotherapy of prostate cancer. *J Nuc Med.* 2015;56(3).
21. Afshar-Oromieh A, Hetzheim H, Kratochwil C, et al. The Theranostic PSMA Ligand PSMA-617 in the Diagnosis of Prostate Cancer by PET/CT: Biodistribution in Humans, Radiation Dosimetry, and First Evaluation of Tumor Lesions. *J Nucl Med.* 2015;56(11):1697-1705.
22. Weineisen M, Schottelius M, Simecek J, et al. 68Ga- and 177Lu-Labeled PSMA I&T: Optimization of a PSMA-Targeted Theranostic Concept and First Proof-of-Concept Human Studies. *J Nucl Med.* 2015;56(8):1169-1176.
23. Heck MM, Retz M, D'Alessandria C, et al. Systemic Radioligand Therapy with 177Lu Labeled Prostate Specific Membrane Antigen Ligand for Imaging and Therapy in Patients with Metastatic Castration Resistant Prostate Cancer. *J Urol.* 2016.
24. Schottelius M, Wirtz M, Eiber M, Maurer T, Wester H-J. [111In]PSMA-I&T: expanding the spectrum of PSMA-I&T applications towards SPECT and radioguided surgery. *EJNMMI Res.* 2015;5(1).
25. Maurer T, Weirich G, Schottelius M, et al. Prostate-specific Membrane Antigen-radioguided Surgery for Metastatic Lymph Nodes in Prostate Cancer. *Eur Urol.* 2015;68(3):530-534.
26. Engfeldt T, Tran T, Orlova A, et al. 99mTc-chelator engineering to improve tumour targeting properties of a HER2-specific Affibody molecule. *Eur J Nucl Med Mol Imaging.* 2007;34(11):1843-1853.
27. Banerjee SR, Pullambhatla M, Foss CA, et al. Effect of Chelators on the Pharmacokinetics of Tc-99m-Labeled Imaging Agents for the Prostate-Specific Membrane Antigen (PSMA). *J Med Chem.* 2013;56(15):6108-6121.
28. Weineisen M, Simecek J, Schottelius M, Schwaiger M, Wester HJ. Synthesis and preclinical evaluation of DOTAGA-conjugated PSMA ligands for functional imaging and endoradiotherapy of prostate cancer. *EJNMMI Res.* 2014;4(1):63.
29. Wang Y, Liu GZ, Hnatowich DJ. Methods for MAG3 conjugation and Tc-99m radiolabeling of biomolecules. *Nat Protoc.* 2006;1(3):1477-1480.
30. Baker RJ, Bellen JC, Fornasiero D, Penglis S. The Preparation of Tc-99m Tertiarybutylisonitrile (Tc-99m-Tbi) by a Method Suitable for Routine Clinical Use. *Nucl Med Biol.* 1986;13(5):527-&.
31. Chen Y, Foss CA, Byun Y, et al. Radiohalogenated prostate-specific membrane antigen (PSMA)-based ureas as imaging agents for prostate cancer. *J Med Chem.* 2008;51(24):7933-7943.
32. Guggenberg EV, Mikolajczak R, Janota B, Riccabona G, Decristoforo C. Radiopharmaceutical development of a freeze-dried kit formulation for the preparation of [99mTc-EDDA-HYNIC-D-Phe1, Tyr3]-octreotide, a somatostatin analog for tumor diagnosis. *J Pharm Sci.* 2004;93(10):2497-2506.
33. Taylor A, Eshima D, Christian PE, Wooten WW, Hansen L, Mcelvany K. Technetium-99m Mag3 Kit Formulation - Preliminary-Results in Normal Volunteers and Patients with Renal-Failure. *J Nucl Med.* 1988;29(5):616-622.
34. Maresca K, Wang JC, Hillier S, et al. Development of a simple kit for Tc-99m-MIP-1404, a single amino acid chelate (SAAC II) derived small molecule inhibitor of prostate specific membrane antigen (PSMA) for imaging prostate cancer. *J Nucl Med.* 2012;53 (suppl. 1):523.
35. Maurer T, Weineisen M, Wester HJ, et al. Psma-Radioguided Surgery: Introducing Molecular Surgery in Patients with Recurrent Prostate Cancer. *J Urol.* 2015;193(4):E1040-E1041.
36. Hillier SM, Maresca KP, Lu G, et al. 99mTc-labeled small-molecule inhibitors of prostate-specific membrane antigen for molecular imaging of prostate cancer. *J Nucl Med.* 2013;54(8):1369-1376.
37. van Oosterom M, Simon H, Mengus L, et al. Revolutionizing (robot-assisted) laparoscopic gamma tracing using a drop-in gamma probe technology. *Am J Nucl Med Mol Imaging.* 2016;6(1):1-17.

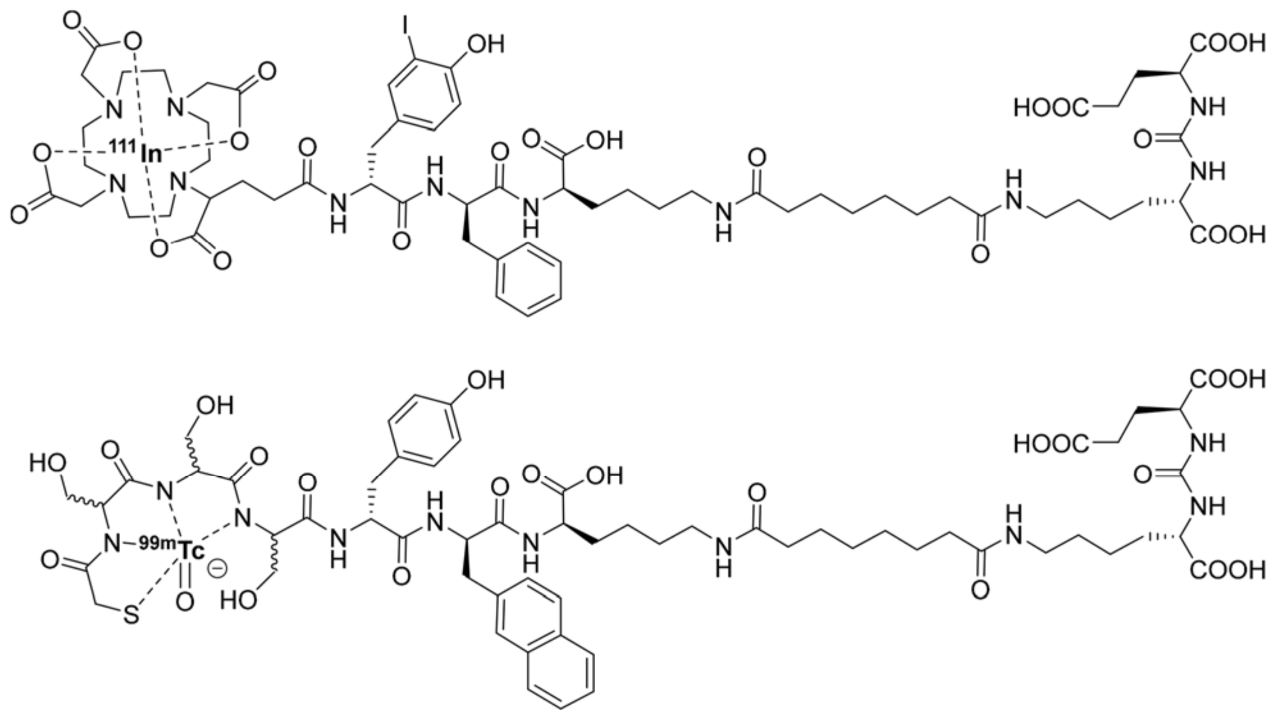

Figure 1 **Chemical structures of ^{111}In-PSMA-I&T and ^{99m}Tc-MAS$_3$/mas$_3$-y-nal-k-Sub-KuE**

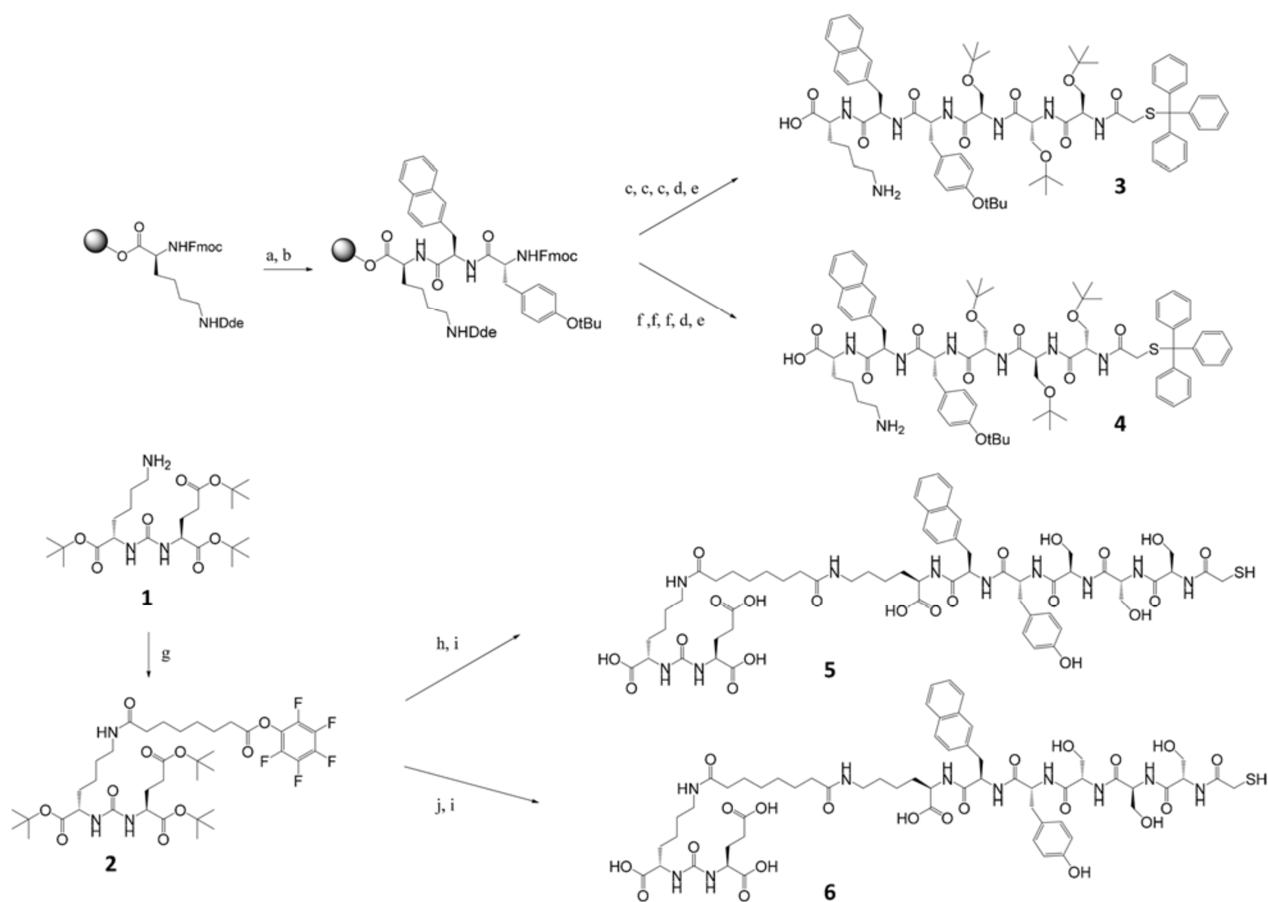

Figure 2 **Synthesis of MAS$_3$-y-nal-k-Sub-KuE (5) and mas$_3$-y-nal-k-Sub-KuE (6, PSMA-I&S)**

(a) 20% piperidine in NMP, Fmoc-D-2Nal-OH, HOBt, TBTU, DIPEA, [NMP]; **(b)** 20% piperidine in NMP, Fmoc-D-Tyr(tBu)-OH, HOBt, TBTU, DIPEA, [NMP]; **(c)** 20% piperidine in NMP, Fmoc-D-Ser(tBu)-OH, HOBt, TBTU, DIPEA, [NMP]; **(d)** 20% piperidine in NMP, S-Trityl-mercaptoacetic acid, HOBt, TBTU, DIPEA, [NMP]; **(e)** DCM/TFE/acetic acid (6/3/1, (v/v)); **(f)** 20% piperidine in NMP, Fmoc-L-Ser(tBu)-OH, HOBt, TBTU, DIPEA, [NMP]; **(g)** Sub(OPfp)$_2$, TEA, [DMF]; **(h) 3,** TEA, [DMF]; **(i)** TFA; **(j) 4**, TEA, [DMF].

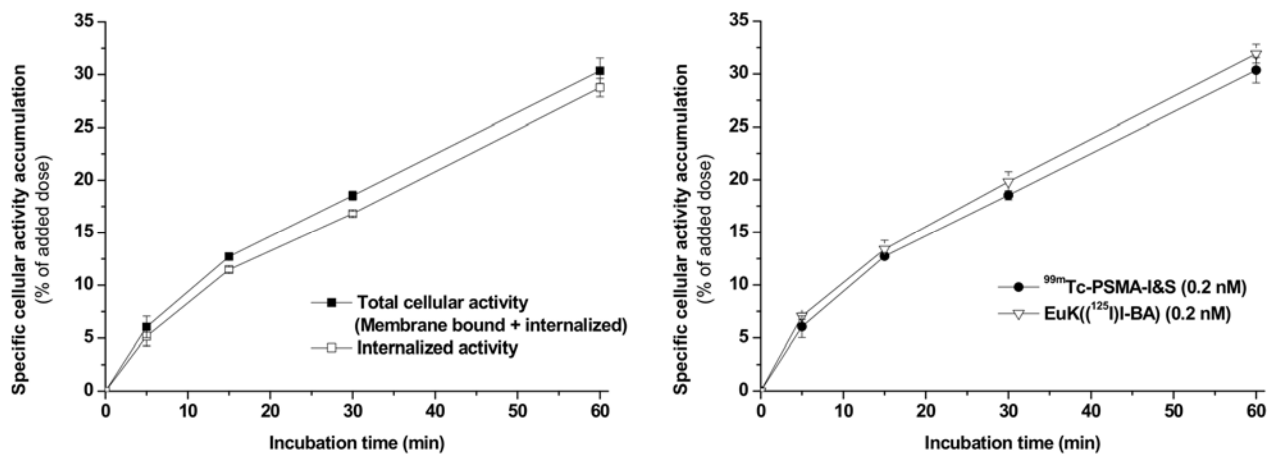

Figure 3 **Left panel**: Kinetics of PSMA-mediated total cellular uptake and internalization of ^{99m}Tc-PSMA-I&S (0.2 nM) into LNCaP cells (37°C) (means±SD (n=3)).

Right panel: Kinetics of PSMA-mediated internalization of ^{99m}Tc-PSMA-I&S (0.2 nM) and the reference (^{125}I-BA)KuE (0.2 nM) into LNCaP cells (37°C) (means±SD (n=3)).

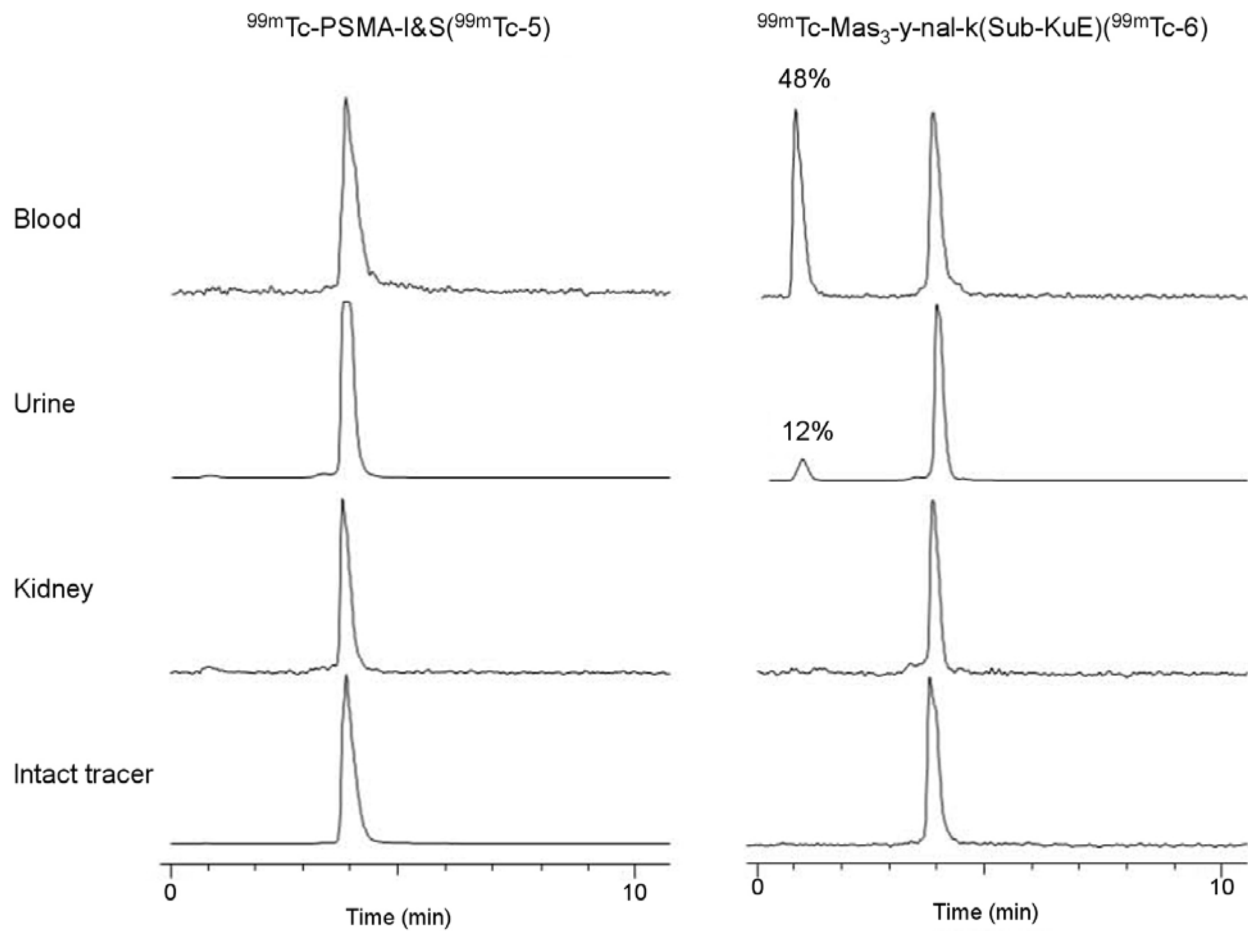

Figure 4 **In vivo stability of ^{99m}Tc-PSMA-I&S and ^{99m}Tc-6 in CD-1 nu/nu mice**

Radio-HPLC chromatograms of intact tracer (before injection) and cell-free blood, urine and kidney homogenate samples collected 1h p.i. of the respective radioligands.

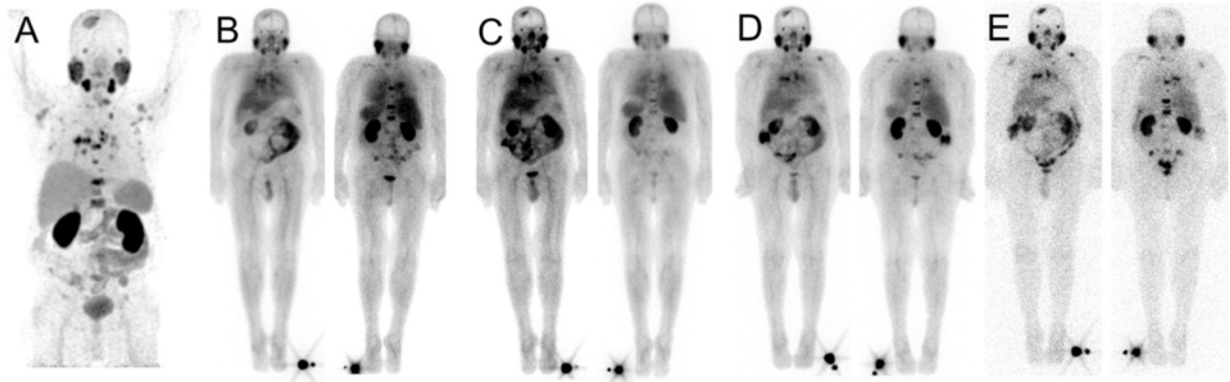

Figure 5 **^{68}Ga-HBED-CC PSMA PET (A) and ^{99m}Tc-PSMA-I&S whole-body planar scintigraphy (B-E)**

PET and planar imaging were carried out in a PCa patient with metastatic, hormone-refractory disease (**A**) ^{68}Ga-HBED-CC PSMA PET, MIP, 1h p.i. (**B-E**). Whole-body planar scintigraphy at 1h (**B**), 3h (**C**), 5h (**D**) and 21h (**E**) p.i. of app. 500 MBq ^{99m}Tc-PSMA-I&S.

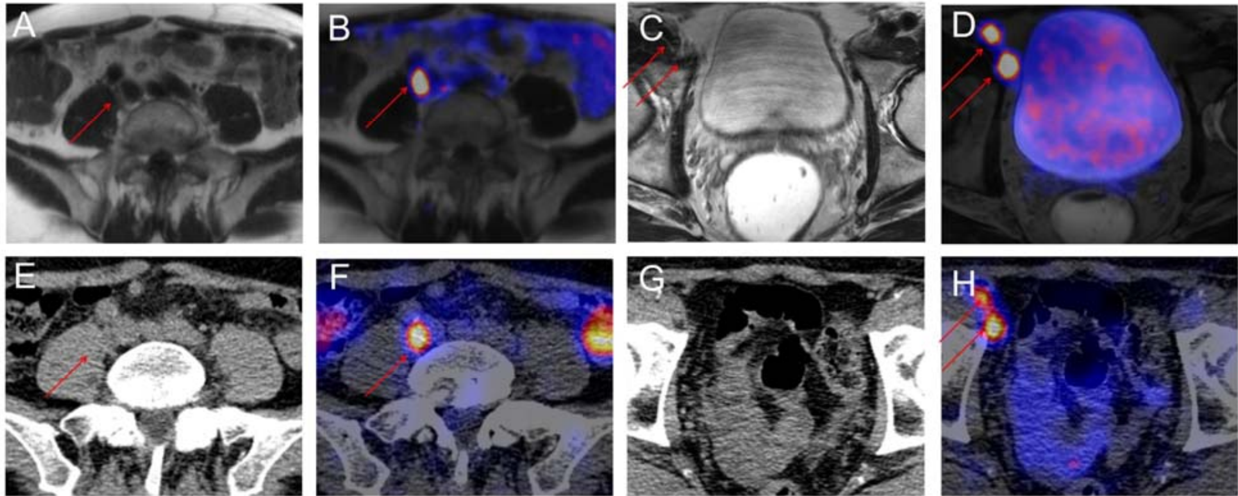

Figure 6 **Preoperative ^{68}Ga-HBED-CC PSMA PET/MR (A-D) and ^{99m}Tc-PSMA-I&S SPECT/CT (E-H)**

^{68}Ga-HBED-CC PSMA PET/MR shows iliac (**A**,**B**) and inguinal lymph node metastases (**C**,**D**). ^{99m}Tc-PSMA-I&S SPECT/CT at 12 h p.i. reveals intense tracer uptake in the same lymph nodes.

Table 1 **PSMA affinities, internalization and lipophilicity of Ga-, Lu- and In-PSMA-I&T (*22, 24*) and of the novel unlabeled and labeled MAS_3/mas_3-y-nal-k(Sub-KuE) analogs**

Ligand	**IC_{50}** (nM)		**Specific internalization** (% of reference)*	**Lipophilicity** (log P_{OW})
Ga-PSMA-I&T	9.4±2.9	^{68}GaPSMA-I&T	59±2	-4.3
Lu-PSMA-I&T	7.9±2.4	^{177}LuPSMA-I&T	76±2	-4.1
In-PSMA-I&T	7.5±1.5	^{111}InPSMA-I&T	104±7	-4.5
mas_3-y-nal-k(Sub-KuE) = PSMA-I&S (**5**)	39.7±1.2	^{99m}TcPSMA-I&S	93±3	-3.0
MAS_3-y-nal-k(Sub-KuE) (**6**)	47.6±2.5	^{99m}Tc-**6**	78±2	-2.9
Re-PSMA-I&S (Re-**5**)	15.5±2.8			
Re-MAS_3-y-nal-k(Sub-KuE) (Re-**6**)	12.4±0.8			

* Specific internalization of the reference compound (^{125}I-BA)KuE was determined in a parallel experiment and used for data normalization

Table 2 **Biodistribution of ^{99m}Tc-PSMA-I&S and the reference ^{111}In-PSMA-I&T (*24*) in LNCaP tumor bearing CB-17-SCID mice at 1h p.i.**
Data are given in %iD/g and are means±SD (n=3-5 animals per group).

	^{111}In-PSMA-I&T	^{99m}Tc-PSMA-I&S	^{99m}Tc-PSMA-I&S + PMPA
Blood	0.24±0.05	1.73±0.50	1.22±0.27
Heart	0.37±0.08	0.94±0.31	0.54±0.12
Lung	1.78±0.18	1.61±0.80	1.20±0.43
Liver	0.26±0.04	1.58±0.24	0.76±0.18
Spleen	47±13	47±17	1.18±0.32
Pancreas	0.59±0.18	0.95±0.19	0.31±0.09
Stomach	0.31±0.16	5.55±0.88	2.64±1.36
Intestines	0.15±0.01	2.46±0.14	2.44±0.33
Kidney	191±24	186±23	9.78±2.95
Muscle	0.19±0.01	0.39±0.15	0.20±0.06
LNCaP tumor	8.07±1.06	8.28±3.27	1.83±0.44